Article

Primary-Side Indirect Control of the Battery Charging Current in a Wireless Power Transfer Charger Using Adaptive Hill-Climbing Control Technique

Abdellah Lassioui [1],[*], Marouane El Ancary [1], Zakariae El Idrissi [1], Hassan El Fadil [1], Kamal Rachid [1] and Aziz Rachid [2]

1   ISA Laboratory, National School of Applied Sciences (ENSA), Ibn Tofail University, Kenitra 14000, Morocco; marouane.elancary@gmail.com (M.E.A.); zakariae.elidrissi@gmail.com (Z.E.I.); elfadilhassan@yahoo.fr (H.E.F.); kamal.rachid01@gmail.com (K.R.)
2   LSIB Laboratory, Faculty of Sciences and Techniques (FST), Hassan II University of Casablanca, Mohammedia 28806, Morocco; rachidaziz03@gmail.com
*   Correspondence: abdellah.lassioui@uit.ac.ma

Abstract: This paper addresses the control task of a wireless power transfer (WPT) charger designed for electric vehicles (EVs). The challenge is to maintain a constant battery charging current when the WPT is controlled on the ground side. Indeed, the intermittent latency involved in the wireless data communication between the ground and vehicle sides leads to system instability. To overcome this issue, a new control approach has been proposed in this paper. The proposed technique ensures indirect control of the battery charging current through control of the current on the ground side. The control technique relies on an adaptive hill-climbing algorithm in conjunction with a PI-based controller. The adaptive parameter is adjusted online, during the operation of the charger, only when a new measure of the battery charging current is received on the primary side. This makes it possible to avoid the need for real-time wireless data communication. It should be noted that this aspect is crucial in ensuring the controller's robustness and stability of the system regardless of potential delays in wireless communication and large misalignments between the coils. The validity of the proposed control technique has been confirmed through simulation. In addition, experimental validation, using a laboratory test bed, demonstrated satisfactory results.

Keywords: electric vehicles; wireless power transfer; battery charging; hill-climbing; indirect control

1. Introduction

Wireless power transfer (WPT) refers to a technique enabling power transfer without physical contact between the electric vehicles (EV) and the charging station [1,2]. It is worth noting that the integration of WPT technology in EVs represents a significant advancement in automotive technology. Indeed, WPT eliminates the need for physical connectors or cables, offering an enhanced and user-centric charging experience for owners of EVs. This can lead to increased adoption of EVs by addressing concerns about charging infrastructure availability and accessibility [3–5].

According to the literature, the WPT technology could be segmented into three categories: static charging mode (for parked vehicles), stationary charging (brief charging stops in urban areas such as bus stops and traffic lights), and dynamic charging (charging while in motion) [6,7]. Static charging, typically using low-power chargers, occurs when the vehicle is stationary in either a private garage or public parking area. Stationary charging briefly boosts EV range without turning off the engine. Dynamic WPT charging occurs while the vehicle is in motion, enabling continuous charging and eliminating the need for frequent stops to recharge [3,4].

The SAE J2954 standard outlines a schematic overview of the WPT charging system which could be divided into two subsystems as shown in Figure 1: a primary side, also

known as ground assembly (GA), and a secondary side known as vehicle assembly (VA). The GA begins with rectifying the AC grid voltage using an AC/DC converter which, guarantees a power factor of unity [8–10]. The rectified DC voltage is supplied to the GA inverter, which operates typically at 85 kHz and is controlled using phase shift techniques [11–13]. A reactive power compensation block follows, eliminating current harmonics and compensating for reactive power [14]. The transmitting coil, powered by the inverter, generates a time-variable magnetic field (MF), transferred wirelessly and guided to the receiving coil via ferrite cores [15,16]. The receiving coil induces an AC voltage, rectified by either controlled or diode-based rectifiers, depending on the system type (bidirectional WPT or unidirectional WPT) [17]. The rectified voltage is used to supply the battery with the recommended charging current and voltage [18–22].
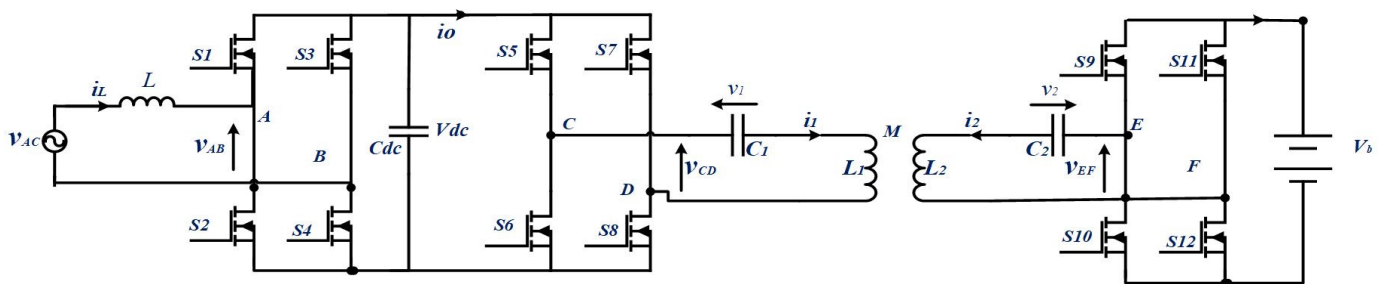

Figure 1. Overall block diagram of a WPT charger.

The SAEJ2954 also covers the interoperability issue in WPT chargers as a crucial aspect for user convenience, safety, and market growth. Indeed, it ensures seamless charging across different brands and models. In addition, interoperability standards also promote safety and protect users from potential hazards. Overall, the interoperability evaluation of WPT chargers can be categorized into three categories: (i) interoperability based on the coil's geometry and parameters, (ii) interoperability based on compensation networks, and (iii) interoperability based on efficiency test [23].

- Interoperability based on the coil's geometry and parameters

In this case, the interoperability is evaluated based on magnetic flux distribution and the coupling coefficient or mutual inductance between the ground side coil and vehicle side coil. Research indicates that circular-circular and circular-rectangular coil pairs generally offer medium coupling coefficients, while DD-DD, Circular-DD and DD-DDQP coil pairs have high mutual coupling and transmission efficiency demonstrating good interoperability [23]. Still, the complex design of these coils could be the main drawback limiting their large adoption in WPT chargers [16].

- Interoperability based on compensation networks

The compensation network in WPT chargers ensures impedance matching and reactive power compensation. Even with interoperable coils, an inappropriate compensation network can cause impedance mismatch, reducing the active power received by the load. Common compensation networks in EV wireless charging include series (S), parallel (P), and LCC. Research shows that only the S-S topology maintains frequency stability despite load changes, indicating why the S-S topology is widely adopted for WPT charging [24].

- Interoperability evaluation based on efficiency test

Evaluating interoperability based on power and efficiency is the most common and intuitive method and is widely used in industries. According to SAE J2954, efficiency is defined as the power ratio from the grid to the battery, which must be at least 85% of the rated working power when the ground and vehicle side coils are perfectly aligned. In addition, the efficiency of the WPT charger must be more than 80% of the maximum misalignment between the coils [25].

For the WPT charger to operate safely and reliably, it is essential to have efficient data communication between the ground assembly and the vehicle assembly. Indeed, in feedback control systems, delayed or inconsistent communication can result in oscillations, overshoot, or even instability of the control loop.

From the control viewpoint, several techniques have been proposed in the literature [26,27]. A ground-side approach is proposed in [28]. The chosen approach prioritizes primary side power regulation to reduce the complexity, size, and cost of vehicle on-board components.

A ground-side control technique of a WPT charger has been proposed in [29]. In this technique, the power transferred to the battery is controlled through the control of DC-DC power converters. The authors claim the universal characteristic of the technique; however, it still suffers from complex power architecture as additional DC-DC converters are used on both sides of the charger. In order to reduce the complexity and size of the WPT charger, a primary-side current and voltage control technique has been proposed in [30]. The technique enables key benefits such as rapid mutual inductance determination, elimination of receiver-side DC-DC converters, and automatic charging mode selection. However, the proposed technique eliminates the use of wireless communication, which is mandatory in a WPT charger as it allows battery state monitoring for safe charging.

Another ground-side technique based on two-level control is proposed in [31]. The proposed technique proves its effectiveness in enhancing the start-up transient time of a WPT charger. Apart from its complexity, the proposed technique is validated using a resistive load which does not model the real behaviour of a real battery.

In [32], the authors propose a charging technique that maintains constant current and voltage using a primary-side controller. This approach utilizes a load identification technique to estimate the battery's equivalent resistance and eliminates the need for real-time wireless communication.

Similar to [32], a primary side control with an improved load identification approach is proposed in [33].

A dual-side communication-free control technique is introduced in [34]. The battery charging current and voltage are controlled using a model predictive control (MPC) technique implemented on the primary side of the WPT charger. However, the complexity and computational burden could be the main limitations of this technique.

The authors in [35] propose a method to simplify the control and eliminate wireless communication. Indeed, the primary side is controlled to limit the output voltage while the secondary side is controlled to achieve CC/CV charging through a DC-DC converter. Besides its simplicity and effectiveness in ensuring good charging performances under large voltage and misalignment variations, this technique suffers from additional power converters and the need for dual-side controllers, which increases its cost and implementation complexity.

The authors in [36,37] propose a simultaneous data and power transfer for a WPT charger. In this technique, both data and power are transmitted through the magnetic coupler using the phase shift keying technique. The proposed method eliminates the need for wireless communication boards; however, additional decoding circuits are mandatory to decode and process data received on the ground side.

From the literature review provided, several common points emerge regarding control techniques for WPT chargers. Indeed, many techniques prioritize primary side power regulation to reduce the complexity, size, and cost of vehicle onboard components by eliminating receiver-side DC-DC converters. While some techniques eliminate the need for wireless communication, it is acknowledged as essential for battery state monitoring for safe charging.

In this paper, the novelty of the proposed technique is that it uses an indirect control of the battery current through the control of the primary side current while maintaining wireless communication between the GA and VA for monitoring and safe operation of the battery charging parameters. The technique is based on an adaptive hill-climbing

algorithm in conjunction with a PI-based controller. The adaptive parameter is updated online, during the operation of the charger, only when a new measure of the battery charging current is available. This makes it possible to avoid the need for real-time wireless data communication. Additionally, it maintains the continuous operation of the controller during the latency intervals.

The structure of this paper is as follows: Section 2 focuses on the modelling of the WPT charger, followed by the presentation of the proposed control technique in Section 3. Section 4 delves into the simulation results, while Section 5 covers the experimental test bed setup and the corresponding results. Section 6 addresses the main results and the supremacy of the proposed control technique over existing methods. Finally, the paper concludes with Section 7.

2. Modelling of the Wireless Power Transfer Charger

This section is devoted to deriving an accurate mathematical model for the WPT charger. This model will be used later for testing the proposed control technique. Note that the modelling task of the AC/DC PFC converter is omitted in this section as the proposed technique is applied only to the DC-DC part of the WPT charger. In addition, the battery has been modelled by an equivalent nonlinear circuit consisting of an open circuit voltage v_{OC} in series with a resistance r_b. Applying Kirchhoff's laws to the circuit in Figure 1 yields (1)–(5):

$$v_{CD} = v_{C1} + L_1 \frac{di_1}{dt} - M \frac{di_2}{dt} \tag{1}$$

$$M \frac{di_1}{dt} = L_2 \frac{di_2}{dt} + v_{C2} + v_{EF} \tag{2}$$

$$i_1 = C_1 \frac{dv_{C1}}{dt} \tag{3}$$

$$i_2 = C_2 \frac{dv_{C2}}{dt} \tag{4}$$

$$i_0 = |i_2| = \frac{v_0 - v_{OC}}{r_b} + C_f \frac{dv_0}{dt} \tag{5}$$

where v_{cd} is the output voltage of the ground side inverter, v_{c1} and v_{c2}, are, respectively, the voltage across the ground and vehicle side compensation capacitors, L_{GA} and L_{VA} are the inductances of the ground and vehicle side coils, i_1 and i_2 are current in the ground side and vehicle side coils, M is the mutual inductance between the coils, v_{ef} and v_0 are, respectively, the voltage at the input and output of the vehicle side rectifier, C_f is the filtering capacitor at the output of the vehicle side rectifier.

Let us select the state variable vector as depicted in (6). Thus, rearranging (1)–(5), one obtains the state space representation of the WPT charger as shown in (7)–(11).

$$x = [v_{C1}, v_{C2}, i_1, i_2, v_0]^T = [x_1, x_2, x_3, x_4, x_5]^T \tag{6}$$

$$\dot{x}_1 = \frac{1}{C_1} x_3 \tag{7}$$

$$\dot{x}_2 = \frac{1}{C_2} x_4 \tag{8}$$

$$\dot{x}_3 = \frac{1}{\rho_1} (v_{CD} - x_1) - \frac{1}{\rho_2} (x_2 - sgn(x_4)x_5) \tag{9}$$

$$\dot{x}_4 = \frac{1}{\rho_2} (v_{CD} - x_1) - \frac{1}{\rho_3} (x_2 - sgn(x_4)x_5) \tag{10}$$

$$\dot{x}_5 = \frac{1}{C_f} sgn(x_4)x_4 - \frac{x_5 - v_{OC}}{C_f r_b} \tag{11}$$

where $\rho_1 = \frac{L_{GA}L_{VA} - M^2}{L_{VA}}$, $\rho_2 = \frac{L_{GA}L_{VA} - M^2}{M}$, $\rho_3 = \frac{L_{GA}L_{VA} - M^2}{L_{GA}}$ and $sgn(x)$ takes 1 when x is >0, -1 when x is negative and 0 when x is null.

The inverter output voltage is a square wave function that could be approximated, as expressed in (12), using the first harmonic approximation. Thus, the expression of the power transferred from the ground side is given in (13).

$$v_{CD} = \frac{4V_{dc}}{\pi} \sin\left(\frac{\phi}{2}\right) \sin(\omega t) \tag{12}$$

where ϕ is the phase shift control signal and V_{dc} is the ground side DC voltage.

Equations (12) and (13) indicate that the amount of power transferred from the primary side to the secondary side could be controlled on the ground side by adjusting the phase shift control signal.

$$P_{GA} = \frac{8}{\pi^2} \frac{V_{dc}V_b}{\omega M} \sin\left(\frac{\phi}{2}\right) \tag{13}$$

It is worth noting that the phase shift control technique is often used in WPT chargers instead of the conventional PWM control technique. The main reason is that the generated output voltage of the ground-side inverter needs to vary at a frequency of 85 kHz. In this case, using the PWM control technique would require a higher carrier frequency ($\gg$ 85 kHz), which involves considerable stress and power switching loss in the ground-side inverter. This is why phase shift control is preferred over PWM in WPT chargers. Indeed, the inverter switching frequency is the same as that of the desired output voltage. A typical driver scheme is illustrated in Figure 2.
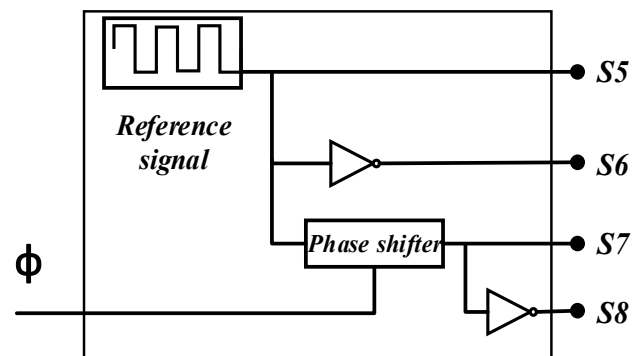

Figure 2. Phase shift driver.

3. Controller Design

This subsection is devoted to designing a controller for the WPT charger. Note that the proposed control approach deals only with the CC charging mode of the battery as it is the most widely adopted in real-life EVs [38]. The main control objective is to ensure a well-regulated battery charging current regardless of the misalignments between the coils and the intermittent communication latencies between the ground side and the vehicle side. It should be noted that the proposed control technique will be implemented on the ground side. This is due to the significant modifications required for implementing these controllers on the vehicle side, as well as the necessity for authorization from the car manufacturer to access the CAN (Controller Area Network).

3.1. Problem Statement

When trying to implement a controller for the WPT charger based on real-time data communication between the ground side and the vehicle side, we noticed an unstable behaviour of the system even if the parameters of the controller were properly tuned. This instability is due to the intermittent latency introduced by the communication boards. Indeed, the ground-side controller performs a periodic check of the received value of the

battery charging current with a period that is mainly fixed by the sampling time of the controller board. As some incontrollable latencies are introduced by wireless communication (based on Wi-Fi as recommended by SAEJ2954 standard [39]), the measured battery charging current value may not be available at the time the controller performs the check. In this case, a maximum of the control signal will be generated leading to an overshoot of the battery current. The opposite scenario occurs when the controller checks the received battery charging current and finds that it is superior to the desired current. In this case, the control signal will be set to its minimum. The repetition of these two scenarios leads to an unstable and oscillating behaviour of the WPT charger. To overcome these issues, a novel control strategy has been proposed in the sequel.

3.2. PI-Based Adaptive Hill-Climbing Controller Design

The general concept of the proposed control approach is illustrated in Figure 3. In this control approach, the battery charging current is controlled indirectly through the control of the average DC on the ground side. Thus, the reference of the average DC $I_{DC,avg,reference}$ is calculated based on the desired battery charging current $I_{Bat,reference}$ as shown in (14):

$$I_{DC,avg,reference} = \frac{I_{Bat,reference} * V_{Bat}}{\eta * V_{DC}} = I_{Bat,reference} * \theta \tag{14}$$
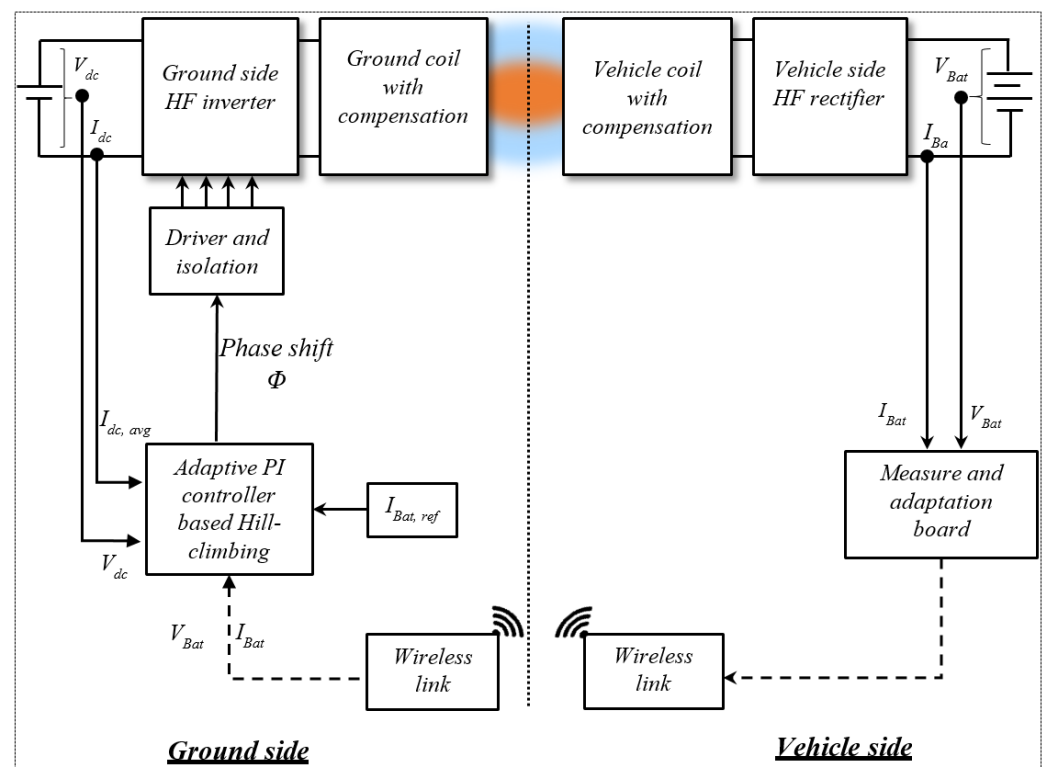
with $\theta = \frac{V_{Bat}}{\eta * V_{DC}}$.

Figure 3. General concept of the proposed control technique.

It is worth noting that the adaptive parameter θ depends on the efficiency η of the charger and the battery voltage V_{Bat} which are subject to change during the charging operation. This parameter will be updated online, during the operation of the charger, only when a new measure of the battery charging current is available. This makes it possible to avoid the need for real-time wireless data communication. Additionally, to maintain the continuous operation of the controller during the latency intervals, introduced by the Wi-Fi communication, the latest calculated value of θ will be used by the controller.

It should be noted that the online adaptation of θ is performed using an adaptive hill-climbing algorithm. Indeed, depending on the sign of the error of the charging current shown in (15), the parameter θ will be either incremented or decremented by a variable step $\Delta\theta$ as in (16). The latter varies as a function of the error as shown in (17). The main advantage of choosing a variable step instead of a fixed one is that it ensures a tight regulation of the battery charging current. Indeed, $\Delta\theta$ decreases as far as the error vanishes, which avoids an overshoot in the battery charging current.

$$e(k) = I_{Bat,ref} - I_{Bat}(k) \tag{15}$$

$$\theta(k) = \theta(k-1) \pm \Delta\theta(k) \tag{16}$$

$$\Delta\theta(k) = \alpha * |e(k)| \tag{17}$$

With $k = 0, 1\ldots N$ is a positive integer and α is a real parameter that will be chosen depending on the desired control performances (rapidity and precision).

Note that the initial value of the adaptive parameter $\theta(0)$ is calculated based on the nominal values of the battery voltage, the efficiency of the WPT charger, and the ground DC voltage.

The flowchart of the proposed adaptive hill-climbing algorithm combined with the PI controller is illustrated in Figure 4.
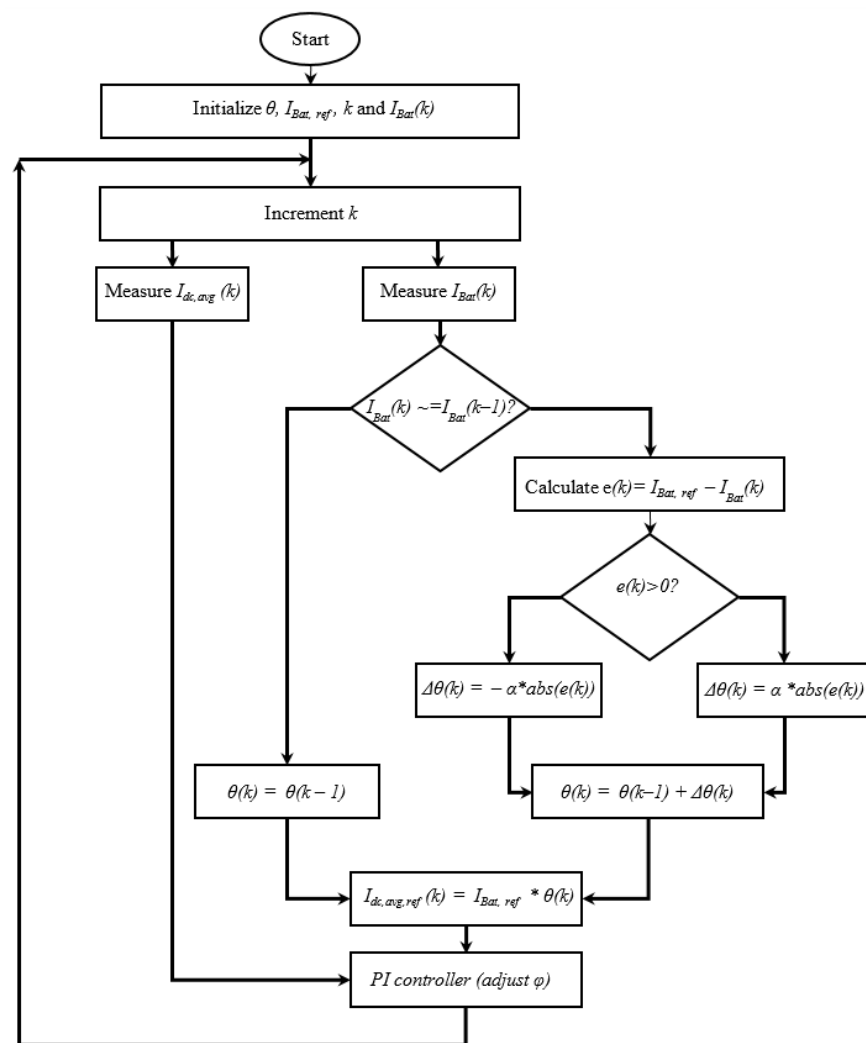

Figure 4. Flowchart of the proposed adaptive hill-climbing algorithm combined with the PI controller.

4. Simulation Results of the Proposed Control Approach

The performances of the control approach have been tested, first using simulation tools. The simulation parameters are listed in Table 1. It should be noted that these parameters are chosen based on those measured in the experimental setup. It is worth noting that The PI controller in our system has been tuned using a trial-and-error approach. This method involved iterative adjustments of the proportional and integral gains to achieve the desired performance in terms of stability, response time, and robustness.

Table 1. Summary of the WPT parameters used during simulation tests.

Parameter	Value
Primary side DC voltage (V_{dc})	120 V
Voltage of the battery (V_{bat})	48 V
Operating frequency (f_{sw})	82.986 kHz
Mutual inductance (M)	44 µH
Ground side coil's inductance L_{GA}	116 µH
Vehicle side coil's inductance L_{VA}	416 µH
Ground side compensation capacitance C_1	8.9 nF
Vehicle side compensation capacitance C_2	31.5 nF
Proportional gain	10
Integral gain	100

The adaptive parameter θ, generated by the hill-climbing algorithm, is plotted in Figure 5. It was initialized by a value of 0.42, which is calculated based on nominal values, namely, an efficiency of 95%, a DC voltage of 120 V, and a battery voltage of 48 V. It is noticed, in the zoomed part of the figure, that θ varies with a variable step ($\Delta\theta$), which takes higher values when the tracking error is larger and small values as far as the tracking error vanishes.
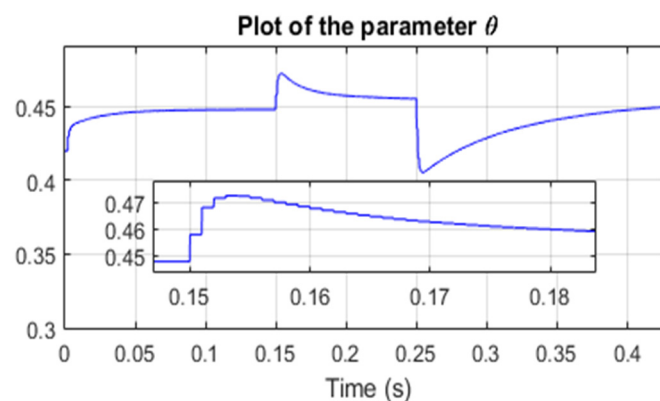

Figure 5. Evolution of the adaptive parameter as a function of time.

Based on the generated θ and the desired battery reference current, an average DC reference current is generated. The latter and the actual average DC are plotted in Figure 6 where it can be seen that the average current reference is dynamically updated based on the desired battery charging current. The figure clearly shows a perfect and smooth tracking of the reference. It follows, according to the indirect control technique, that the battery charging current is well-regulated to the desired value. This could be verified as shown in Figure 7, where we plotted the battery charging current and its reference. The latter was stepped up from 2 A to 3 A at 0.15 s and stepped down again to 1 A at 0.25 s. One can see

that all the desired battery charging currents have been reached with a convergence time of less than 0.1 s.
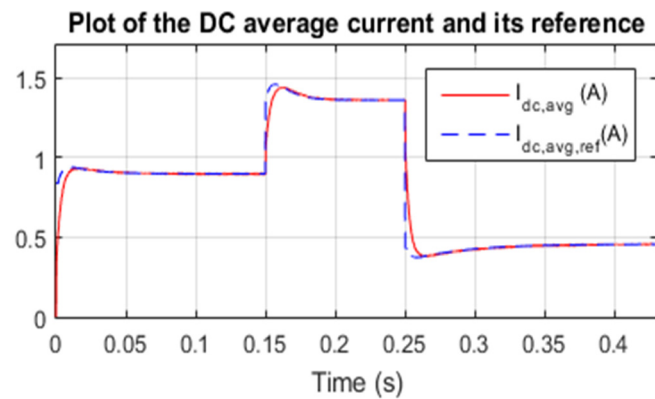

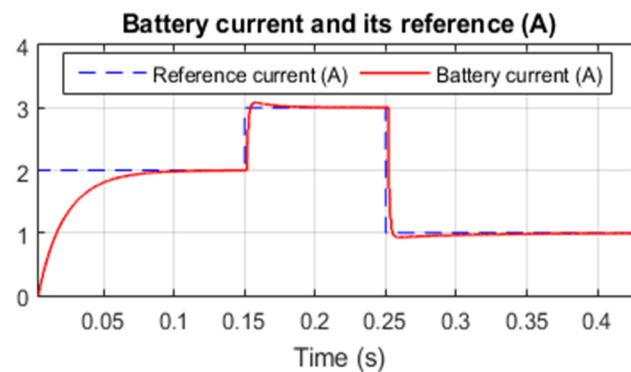**Figure 6.** Evolution of the average DC and its reference.

Figure 7. Plot of the battery charging current and its reference during simulation test.

The phase shift control signal, generated by the PI controller, is plotted in Figure 8. We can see that the latter evolves smoothly without any saturation. This helps reduce the stress and ensures optimal working of the power converters.
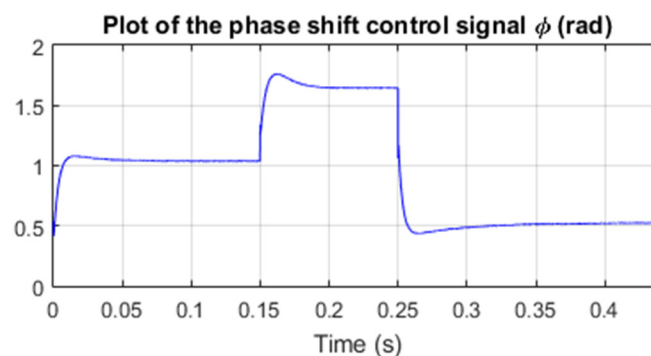

Figure 8. Evolution of the phase shift control signal as a function of time.

Figure 9 shows the evolution of the battery voltage as a function of the charging current. We notice a small increase in the voltage around the nominal value of 48 V when the battery is being charged.
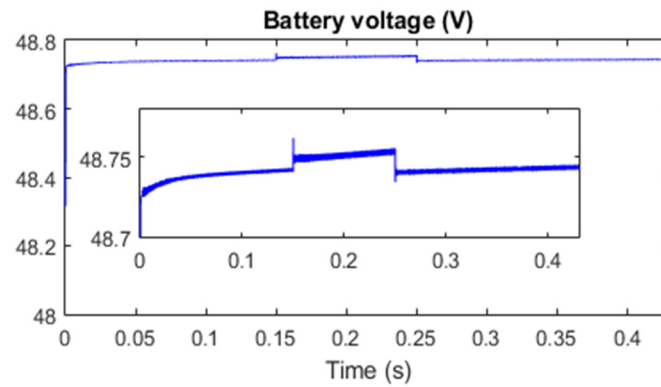
Figure 9. Evolution of the battery voltage.

The inverter output voltage and current are plotted in Figure 10. The zoomed parts of the figure (Figure 10a,b) show that the power transferred from the ground side to the vehicle side is adjusted by changing the RMS value of the voltage through the phase shift control signal. It is also evident that the shape of the primary coil's current looks like a sine wave despite the voltage being a square wave with infinite harmonics. This is due to the filtering behaviour of the resonant LC network (ground side coil with its associated compensation series capacitor) tuned at the operating frequency.
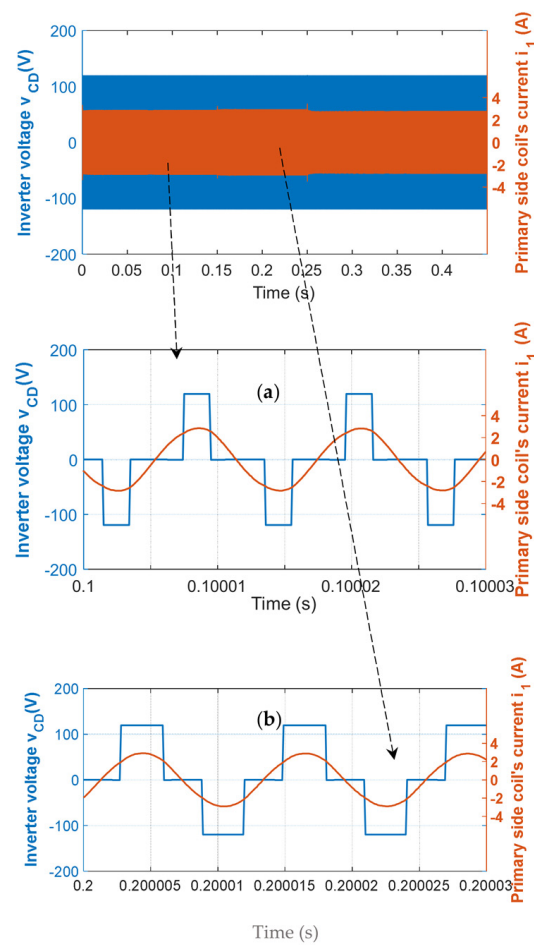

Figure 10. Inverter output voltage and primary side coil's current, (**a**) zoom at time 0.1 s and (**b**) zoom at 0.2 s.

The vehicle side rectifier input voltage and the coil's current are plotted in Figure 11. The voltage is a square wave with a maximum value that is fixed by the actual battery

voltage. However, due to the filtering behaviour of the vehicle side LC network, the current is a sine wave with a frequency of 85 kHz. We notice that both of these signals are in phase with variations in the coil's current as a function of the desired battery charging current.
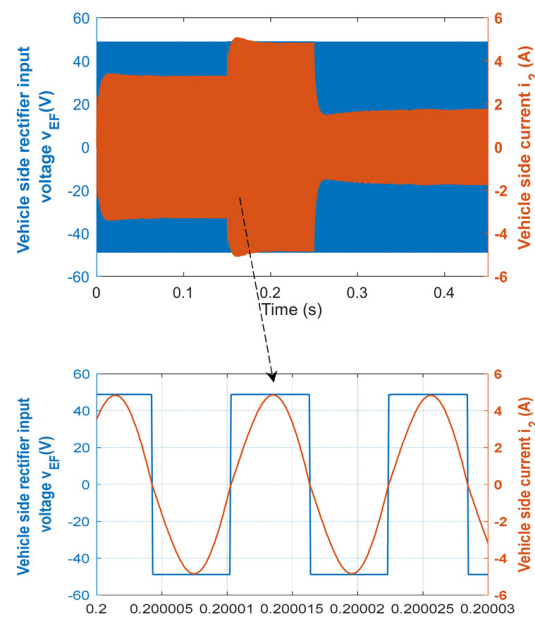

Figure 11. Voltage at the rectifier input and vehicle side coil's current with a zoom at time 0.2 s.

The obtained simulation results show that all the desired control objectives have been realized, which verifies the efficacy of the PI-based adaptive hill-climbing control technique.

5. Experimental Results of the Proposed Control Approach

5.1. Description of the Laboratory Test Bed

To validate the efficacy of the proposed control technique, a test setup was constructed. It is worth noting that Silicon Carbide (SiC) and Galium Nitride (GaN) MOSFET-based power converters are emerging technologies best suited for WPT chargers. Indeed, their performances remain higher even when operating at high frequency and high power. SiC MOSFET technology is adopted in the present paper (reference CRD 8FF1217P-1 from Wolfspeed, Inc., Durham, NC, USA).

To minimize the proximity and skin effect, the GA and VA coils are made of 1050-strand twisted Litz wire. In addition, Mn–Zn ferrite cores (from TDK Corporation, Japan) are also added to guide the flux between the coils.

From a design viewpoint, key parameters for a circular planar coil include the inner radius, the outer radius, the spacing between the turns, and the number of turns. These must be carefully selected to achieve the desired performance. It is worth noting that increasing the spacing between turns can help achieve the desired inductance with fewer turns, reducing the coil's weight and cost. However, it also decreases mutual coupling. To ensure better coupling, turns are brought closer together to eliminate spacing, leaving the number of turns and the inner and outer radii as the primary adjustable parameters for desired coil performance.

The ground-side coil has an outer diameter of 48 cm. It is worth noting that the outer diameter is kept constant to ensure proper coupling at a nominal air gap of 12 cm, as the height of the created magnetic flux is approximately one-quarter of the outer diameter of the coil. The inner diameter has been adjusted to 5.5 cm to achieve the desired coil inductance in conjunction with the compensation capacitor to ensure resonance operation. In addition, the number of spires is 40, leading to an inductance of 416 μH with six ferrite bars.

The geometry for the vehicle-side coil has an outer diameter of 30 cm and an inner diameter of 8.5 cm. The smaller outer diameter, compared to that of the ground-side coil,

ensures that the vehicle-side coil remains within the coverage area of the ground-side coil, even in the presence of large misalignments, in order to ensure good coupling and keep the power transfer efficiency as high as possible. Once again, the inner diameter is adjusted to ensure the desired coil inductance to ensure the resonance operation in conjunction with the compensation capacitors. Note that, with this configuration, 19 spires, and 4 ferrites bars, the obtained inductance value of the ground side coil is 116 µH.
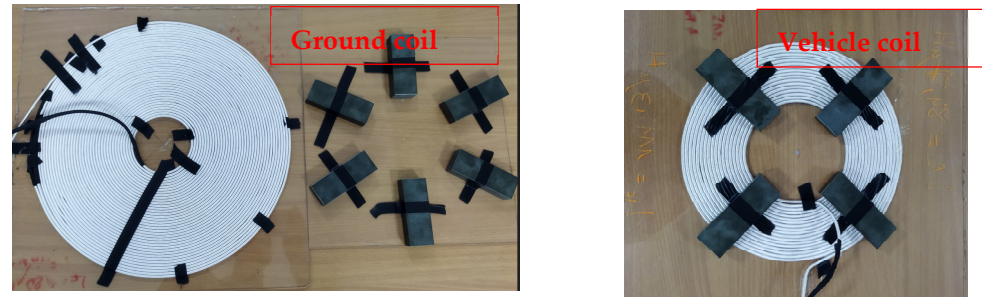
Figure 12 illustrates the realized coils.

Figure 12. Image of the ground-side coil and the vehicle-side coil.

The series compensation topology, which consists of adding capacitors in series with the coils, is used in our case. The main advantage of series compensation is that the calculated capacitor values are independent of the mutual inductance between the coils. This is generally desired in WPT chargers as misalignments lead to variable mutual coupling. Still, one issue with this compensation topology is the high voltage involved across the capacitors, which complicates the design task. Indeed, several capacitors are connected in series, forming a branch, to withstand the involved high voltage. Then, several branches could be connected in parallel to achieve the desired capacitance value. The realized ground side (8.9 nF) and vehicle side (31.5 nF) compensation boards are illustrated in Figure 13.

Figure 13. Compensation boards. Ground side (**left**) and ground side (**right**).

It is worth noting that the operating frequency is calculated based on the realized compensation capacitors and coils. Indeed, the capacitance values of the compensation boards on the ground and vehicle sides are C1 = 8.9 nF and C2 = 31.5 nF, respectively. In addition, the inductances of the coils on the ground and vehicle sides are L1 = 416 µH and L2 = 116 µH, respectively. These values result in two resonance frequencies: f1 = 82,713 Hz and f2 = 83,259 Hz. Therefore, the resonance frequency is chosen as the mean value of f1 and f2, which is f = (f1 + f2)/2 = 82,986 Hz. Note that this frequency falls within the recommended range of the SAE J2954 standard (81–91 kHz).

The air-gap distance between the coils is set to 125 mm (nominal distance of the Z1 class of the SAEJ2954 standard). This air-gap distance gives rise to a mutual coupling of 44 µH between the coils. As for the control board, TI C2000 f28335 (from Texas Instrument, Texas, USA) is used. Raspberry Pi4 is used to ensure Wi-Fi communication between the ground and vehicle parts of the WPT charger. In addition, MicroLabBox (from dSPACE

GmbH, Paderborn Germany) and measurement boards are used for data acquisition and logging. Moreover, a 48 V battery pack is used to emulate the vehicle's battery. The detailed realization of the prototype can be found in [40]. Figure 14 illustrates the realized prototype.

Figure 14. The experimental testbed used for testing the control approach.

5.2. Experimental Results

The performances of the proposed control technique are tested experimentally using two coil positions. In the first positioning, the two coils are laterally misaligned ($\Delta x = \Delta y = 5$ cm) and spaced at a distance of 12 cm. In the second positioning, the air gap was increased to 15 cm in the presence of large misalignments ($\Delta x = \Delta y = 10$ cm), which are above the testing limits of the SAEJ2954 standard. The aim is to test the controller under extreme conditions. The results obtained for each scenario are presented in the sequel.

Starting with the first scenario, the battery charging current and its reference are plotted in Figure 15. The desired current was set first to 1 A then stepped up to 3 A and down to 2 A, 1 A, and 0 A. The point is to check the tracking performances of the controller for different values of the charging current. As illustrated, all the desired reference currents are reached without any overshoot, which proves the effectiveness of the proposed control technique. The average DC is plotted in Figure 16 where it can be seen that it steps up and down as a function of the variations in the battery current.
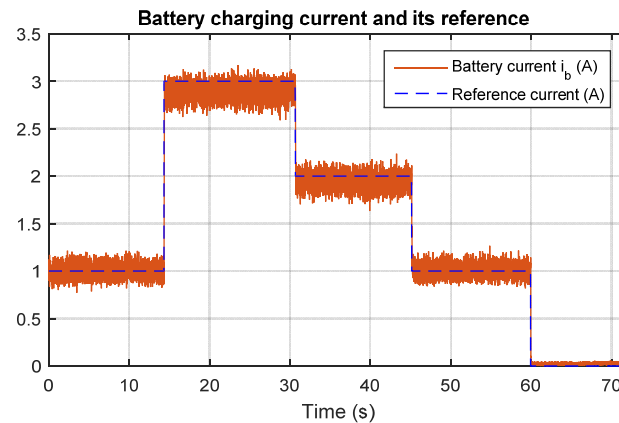

Figure 15. Evolution of the battery charging current and its reference.
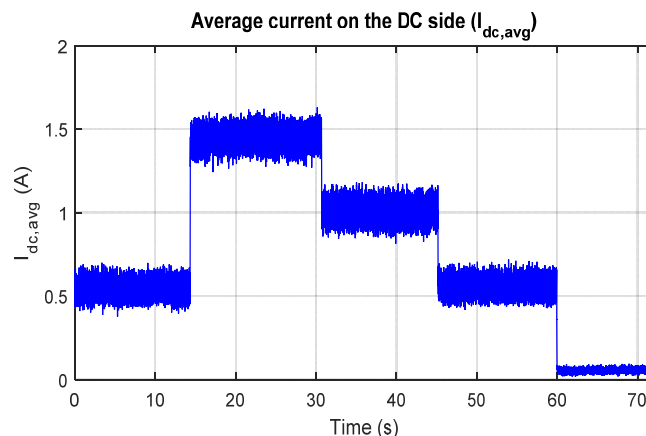

Figure 16. Evolution of the average DC on the primary side.

The DC side and battery voltages are plotted in Figures 17 and 18. Thus, the calculation, using the values of the currents and voltages on both sides, shows that the efficiency of the WPT charger varies according to the power transferred to the battery. Indeed, when the battery charging current is set to 1 A, the corresponding battery voltage, DC side voltage and DC side current are, respectively, 51 V, 120 V, and 0.5 A. These values give rise to an efficiency of approximately 85%. Similarly, the power transfer efficiencies corresponding to the case where the battery charging currents are set to 3 A and 2 A are, respectively, 90% and 87%. These results show that the efficiency varies according to the power transferred to the battery. Indeed, the efficiency increases as the power transferred increases. In addition, these results prove the effectiveness of the adaptive control technique in maintaining the battery charging currents at the desired values despite the power transfer efficiency variations.
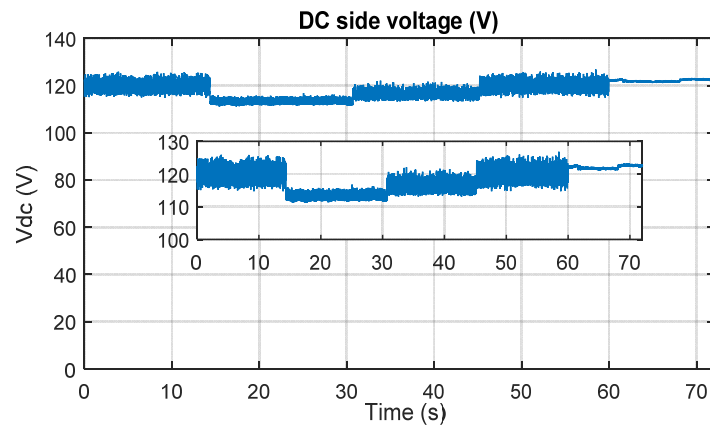
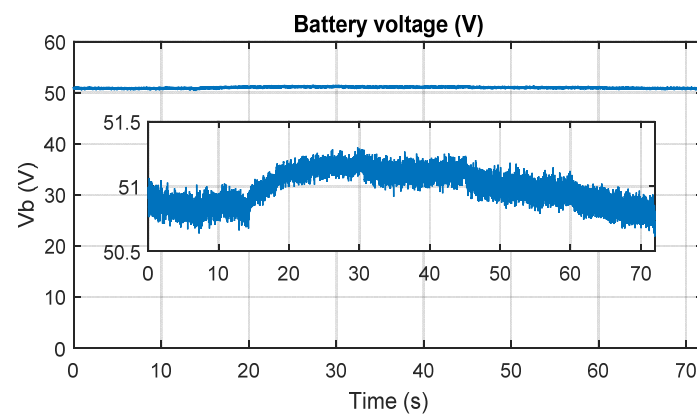**Figure 17.** Evolution of the DC voltage on the primary side.

Figure 18. Plot of the battery voltage.

Moving to the second scenario, the efficiency of the WPT charger is expected to be lower than that of the first scenario as the coils are largely misaligned and the air gap is increased. The positioning of the primary and secondary coils is illustrated in Figure 19.
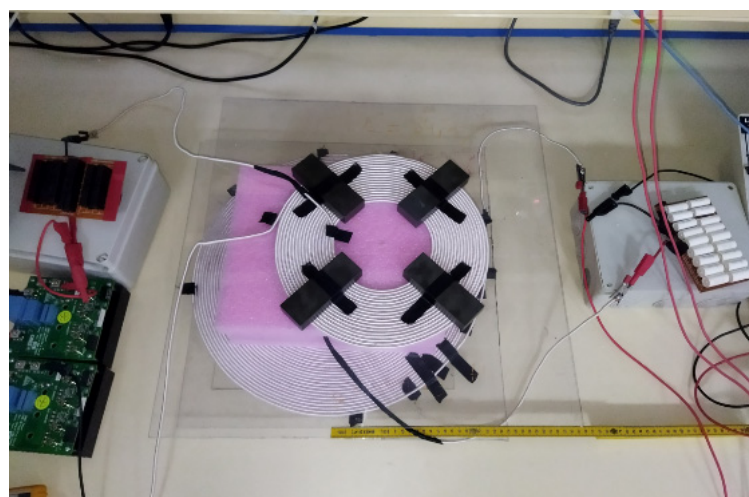

Figure 19. Image of the primary (**bottom**) and secondary (**top**) coils under large misalignments and air gaps.

During this test, as shown in Figure 20, the battery reference current is first set to 2 A, stepped up to 3 A, and then stepped down to 1 A and 0 A. In the same figure, one can see

that the actual battery charging current tracks these references well, despite the fact that the test is performed considering the worst positioning scenario of the coils.
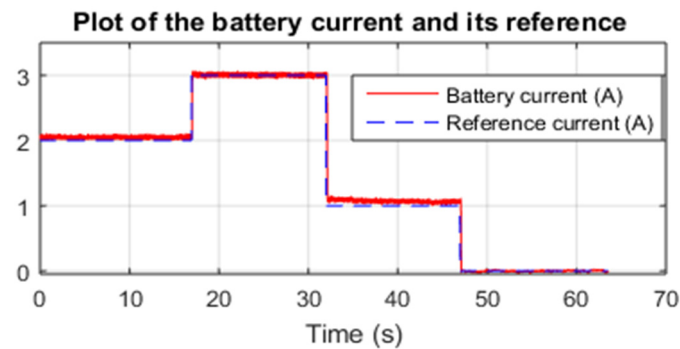

Figure 20. Plot of the battery current and its reference during the second testing scenario.

The corresponding average DC is plotted in Figure 21, where it can be seen that it varies according to the changes in the battery current.
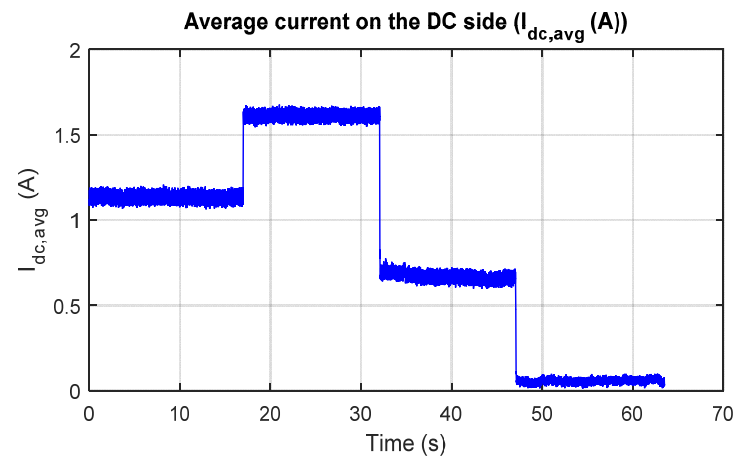

Figure 21. Plot of the average current on the primary side during the second testing scenario.

In addition, considering the voltages on the battery side and the DC side, plotted in Figures 22 and 23, and the currents in the DC side and battery side show that the efficiency in this scenario drops to approximately 75%. This test reveals that the proposed control technique has good performance even in the presence of large air gaps and misalignments between the coils. In addition, the system exhibits good stability against communication latency.
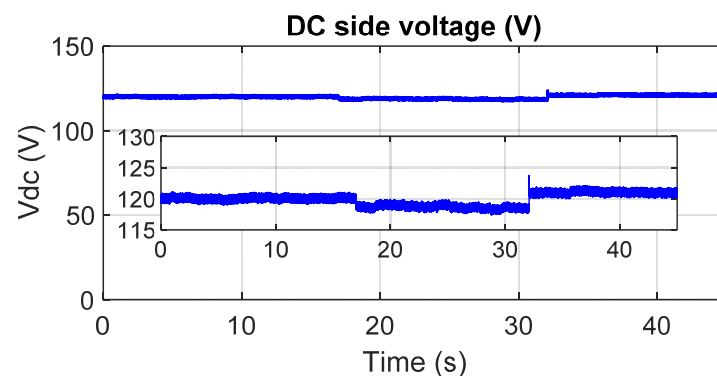

Figure 22. Plot of the DC voltage on the primary side during the second testing scenario.
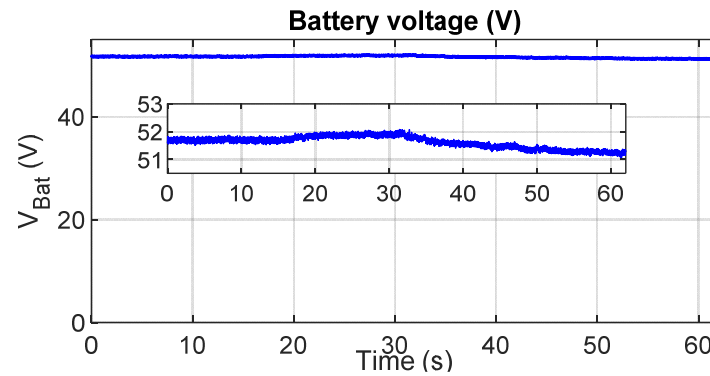
Figure 23. Plot of the battery voltage during the second testing scenario.

6. Results, Discussion, and Performance Evaluation of the Proposed Control Technique

The novelty of our proposed technique lies in its indirect control of the battery current through the regulation of the primary side current while maintaining wireless communication between the ground assembly (GA) and vehicle assembly (VA) for monitoring and safe operation of the battery charging current. This technique utilizes an adaptive hill-climbing algorithm in conjunction with a PI-based controller. The adaptive parameter is updated online during charger operation, only when a new measurement of the battery charging current is available. This approach avoids the need for real-time wireless data communication and ensures continuous controller operation during latency intervals.

The obtained simulation and experimental results illustrate the successful application of the proposed control technique. Thus, the experimental validation confirms the control technique's robustness under real-world conditions, including significant misalignments and varied air gaps. The main results are summarized as follows:

- Adaptive parameter (θ) behaviour

The adaptive parameter θ is dynamically adjusted based on the tracking error. Larger steps occur with significant errors and smaller steps as errors decrease, ensuring adaptive system stability and efficient performance.

- Accurate and robust current tracking

Both the average DC and the battery charging current closely follow their respective references, even during current steps, indicating the controller's precision in maintaining desired charging currents. In addition, in scenarios with both moderate ($\Delta x = \Delta y = 5$ cm, 12 cm air gap) and large misalignments ($\Delta x = \Delta y = 10$ cm, 15 cm air gap), the battery charging current accurately tracks the reference values without overshoot, highlighting the controller's robustness and stability.

- Smooth control signal

The phase shift control signal evolves smoothly without saturation, minimizing stress on power converters and ensuring optimal operation.

- Adaptive Power transfer

The average DC is adjusted effectively in response to changes in the battery current, validating the indirect control approach.

It is worth noting that, from the literature review given in the introduction section, it was found that several common points emerge regarding control techniques for WPT chargers. Many techniques prioritize primary-side power regulation to reduce the complexity, size, and cost of vehicle onboard components by eliminating receiver-side DC-DC converters. While some methods eliminate the need for wireless communication, it remains essential for monitoring battery current to ensure safe charging.

Compared to existing techniques, our approach not only maintains the essential wireless communication for battery state monitoring but also achieves stable and efficient

charging control. This combination of indirect battery current control and adaptive algorithmic adjustments enhances the reliability and performance of WPT chargers, addressing the limitations identified in the literature.

7. Conclusions

This paper addresses the critical control task of wireless power transfer (WPT) chargers for electric vehicles (EVs), focusing on maintaining a stable battery charging current amidst challenges such as coil misalignment and intermittent communication latencies between the ground and vehicle sides. The paper introduces a novel control approach that employs a combination of a hill-climbing algorithm and a PI controller, enabling indirect control of the battery charging current through the ground-side current control.

The proposed technique ensures the continuous and stable operation of the controller, effectively mitigating the impact of wireless communication latencies. By leveraging an adaptive parameter updated online during charger operation, we circumvent the need for real-time wireless data communication, thus enhancing system robustness and stability regardless of potential delays and large coil misalignments.

Simulation and experimental validation on a laboratory test bed confirm the effectiveness and robustness of our proposed approach, even under worst-case testing scenarios. The obtained results validate the viability of the proposed technique for real-world applications.

For future work, the focus will be on further optimization and validation of the proposed technique under diverse operating conditions, including the use of different coil designs and compensation topologies. Additionally, we intend to incorporate battery parameter estimation to further enhance the reliability and performance of the proposed control technique.

References

1. Lukic, S.M.; Pantic, Z. Cutting the Cord: Static and Dynamic Inductive Wireless Charging of Electric Vehicles. *Electrif. Mag. IEEE* **2013**, *1*, 57–64. [CrossRef]
2. Patil, D.; McDonough, M.K.; Miller, J.M.; Fahimi, B.; Balsara, P.T. Wireless Power Transfer for Vehicular Applications: Overview and Challenges. *IEEE Trans. Transp. Electrific.* **2018**, *4*, 3–37. [CrossRef]
3. Laha, A.; Kalathy, A.; Pahlevani, M.; Jain, P. A Comprehensive Review on Wireless Power Transfer Systems for Charging Portable Electronics. *Eng* **2023**, *4*, 1023–1057. [CrossRef]
4. Lassioui, A.; Fadil, H.E.; Rachid, A.; Belhaj, F.Z.; Tarkany, O.; Bajit, A. Characterestics Analysis of Wireless Power Transfer System for Electric Vehicle Charging Applications. In Proceedings of the 2018 International Symposium on Advanced Electrical and Communication Technologies (ISAECT), Rabat, Morocco, 21–23 November 2018; pp. 1–6.
5. Li, S.; Mi, C.C. Wireless Power Transfer for Electric Vehicle Applications. *IEEE J. Emerg. Sel. Top. Power Electron.* **2015**, *3*, 4–17. [CrossRef]
6. Machura, P.; De Santis, V.; Li, Q. Driving Range of Electric Vehicles Charged by Wireless Power Transfer. *IEEE Trans. Veh. Technol.* **2020**, *69*, 5968–5982. [CrossRef]
7. Zaid, S.A.; Albalawi, H.; Alatwi, A.M.; Elemary, A. Performance Improvement of an Electric Vehicle Charging Station Using Brain Emotional Learning-Based Intelligent Control. *Processes* **2024**, *12*, 1014. [CrossRef]
8. Huang, Q.; Huang, A.Q. Review of GaN Totem-Pole Bridgeless PFC. *CPSS Trans. Power Electron. Appl.* **2017**, *2*, 187–196. [CrossRef]
9. Bentalhik, I.; El Fadil, H.; Lassioui, A.; Koundi, M.; El Idrissi, Z.; Giri, F. Adaptive Observer Design for a Bidirectional AC/DC Totem Pole PFC Power Converter. *IFAC-PapersOnLine* **2022**, *55*, 438–443. [CrossRef]

10. Mounica, M.; Rajpathak, B.A.; Kolhe, M.L.; Naik, K.R.; Moparthi, J.R.; Kotha, S.K. Piece-Wise Droop Controller for Enhanced Stability in DC-Microgrid-Based Electric Vehicle Fast Charging Station. *Processes* **2024**, *12*, 892. [CrossRef]

11. Berger, A.; Agostinelli, M.; Vesti, S.; Oliver, J.A.; Cobos, J.A.; Huemer, M. A Wireless Charging System Applying Phase-Shift and Amplitude Control to Maximize Efficiency and Extractable Power. *IEEE Trans. Power Electron.* **2015**, *30*, 6338–6348. [CrossRef]

12. Li, Y.; Hu, J.; Chen, F.; Li, Z.; He, Z.; Mai, R. Dual-Phase-Shift Control Scheme With Current-Stress and Efficiency Optimization for Wireless Power Transfer Systems. *IEEE Trans. Circuits Syst. I Regul. Pap.* **2018**, *65*, 3110–3121. [CrossRef]

13. Lassioui, A.; Fadil, H.E.; Rachid, A.; El-Idrissi, Z.; Bouanou, T.; Belhaj, F.Z.; Giri, F. Modelling and Sliding Mode Control of a Wireless Power Transfer System for BEV Charger. *Int. J. Model. Identif. Control* **2020**, *34*, 171–186. [CrossRef]

14. Mohamed, A.A.S.; Berzoy, A.; de Almeida, F.G.N.; Mohammed, O. Modeling and Assessment Analysis of Various Compensation Topologies in Bidirectional IWPT System for EV Applications. *IEEE Trans. Ind. Appl.* **2017**, *53*, 4973–4984. [CrossRef]

15. Bouanou, T.; Fadil, H.E.; Lassioui, A. Analysis and Design of Circular Coil Transformer in a Wireless Power Transfer System for Electric Vehicle Charging Application. In Proceedings of the 2020 International Conference on Electrical and Information Technologies (ICEIT), Rabat, Morocco, 4–7 March 2020; pp. 1–6.

16. Bouanou, T.; El Fadil, H.; Lassioui, A.; Assaddiki, O.; Njili, S. Analysis of Coil Parameters and Comparison of Circular, Rectangular, and Hexagonal Coils Used in WPT System for Electric Vehicle Charging. *World Electr. Veh. J.* **2021**, *12*, 45. [CrossRef]

17. Rachid, A.; El Fadil, H.; Gaouzi, K.; Rachid, K.; Lassioui, A.; El Idrissi, Z.; Koundi, M. Electric Vehicle Charging Systems: Comprehensive Review. *Energies* **2023**, *16*, 255. [CrossRef]

18. Rachid, A.; Fadil, H.E.; Giri, F. Dual Stage CC-CV Charge Method for Controlling DC-DC Power Converter in BEV Charger. In Proceedings of the 2018 19th IEEE Mediterranean Electrotechnical Conference (MELECON), Marrakech, Morocco, 2–7 May 2018; pp. 74–79.

19. Lassioui, A.; EL Fadil, H.; Rachid, A.; Bouanou, T.; Giri, F. Adaptive Output Feedback Nonlinear Control of a Wireless Power Transfer Charger for Battery Electric Vehicle. *J. Control Autom. Electr. Syst.* **2021**, *32*, 492–506. [CrossRef]

20. Jia, Q.-S.; Long, T. A Review on Charging Behavior of Electric Vehicles: Data, Model, and Control. *Control Theory Technol.* **2020**, *18*, 217–230. [CrossRef]

21. Wu, W.; Zeng, J.; Jian, Q.; Tang, L.; Hou, J.; Han, C.; Song, Q.; Luo, Y. A Li-Ion Battery State of Charge Estimation Strategy Based on the Suboptimal Multiple Fading Factor Extended Kalman Filter Algorithm. *Processes* **2024**, *12*, 998. [CrossRef]

22. Zhang, R.; Li, X.; Sun, C.; Yang, S.; Tian, Y.; Tian, J. State of Charge and Temperature Joint Estimation Based on Ultrasonic Reflection Waves for Lithium-Ion Battery Applications. *Batteries* **2023**, *9*, 335. [CrossRef]

23. Song, K.; Lan, Y.; Zhang, X.; Jiang, J.; Sun, C.; Yang, G.; Yang, F.; Lan, H. A Review on Interoperability of Wireless Charging Systems for Electric Vehicles. *Energies* **2023**, *16*, 1653. [CrossRef]

24. Triviño, A.; González-González, J.M.; Aguado, J.A. Wireless Power Transfer Technologies Applied to Electric Vehicles: A Review. *Energies* **2021**, *14*, 1547. [CrossRef]

25. Venkatesan, R.; Savio, A.D.; Balaji, C.; Narayanamoorthi, R.; Kotb, H.; ELrashidi, A.; Nureldeen, W. A Comprehensive Review on Efficiency Enhancement of Wireless Charging System for the Electric Vehicles Applications. *IEEE Access* **2024**, *12*, 46967–46994. [CrossRef]

26. Nguyen, H.T.; Alsawalhi, J.Y.; Hosani, K.A.; Al-Sumaiti, A.S.; Jaafari, K.A.A.; Byon, Y.-J.; Moursi, M.S.E. Review Map of Comparative Designs for Wireless High-Power Transfer Systems in EV Applications: Maximum Efficiency, ZPA, and CC/CV Modes at Fixed Resonance Frequency Independent From Coupling Coefficient. *IEEE Trans. Power Electron.* **2022**, *37*, 4857–4876. [CrossRef]

27. Sagar, A.; Kashyap, A.; Nasab, M.A.; Padmanaban, S.; Bertoluzzo, M.; Kumar, A.; Blaabjerg, F. A Comprehensive Review of the Recent Development of Wireless Power Transfer Technologies for Electric Vehicle Charging Systems. *IEEE Access* **2023**, *11*, 83703–83751. [CrossRef]

28. Miller, J.M.; Onar, O.C.; Chinthavali, M. Primary-Side Power Flow Control of Wireless Power Transfer for Electric Vehicle Charging. *IEEE J. Emerg. Sel. Top. Power Electron.* **2015**, *3*, 147–162. [CrossRef]

29. Baros, D.; Rigogiannis, N.; Drougas, P.; Voglitsis, D.; Papanikolaou, N.P. Transmitter Side Control of a Wireless EV Charger Employing IoT. *IEEE Access* **2020**, *8*, 227834–227846. [CrossRef]

30. Yang, Y.; Zeng, J.; Hui, S.Y.R. A Fast Primary-Side Current and Voltage Control for Direct Wireless Battery Chargers. *IEEE J. Emerg. Sel. Top. Power Electron.* **2024**, *12*, 355–366. [CrossRef]

31. Shi, W.; Deng, J.; Wang, Z.; Cheng, X. The Start-up Dynamic Analysis and One Cycle Control-PD Control Combined Strategy for Primary-Side Controlled Wireless Power Transfer System. *IEEE Access* **2018**, *6*, 14439–14450. [CrossRef]

32. Song, K.; Li, Z.; Jiang, J.; Zhu, C. Constant Current/Voltage Charging Operation for Series–Series and Series–Parallel Compensated Wireless Power Transfer Systems Employing Primary-Side Controller. *IEEE Trans. Power Electron.* **2018**, *33*, 8065–8080. [CrossRef]

33. Liu, Z.; Wang, L.; Guo, Y.; Li, S. Primary-Side Linear Control for Constant Current/Voltage Charging of the Wireless Power Transfer System Based on the LCC-N Compensation Topology. *IEEE Trans. Ind. Electron.* **2022**, *69*, 8895–8904. [CrossRef]

34. Kalat, S.N.; Vaez-Zadeh, S.; Zakerian, A.; Babaki, A.; Ebel, T. A Communication-Free and Model-Free Predictive Control for a Dynamic IPT System With High Power Factor for Electric Vehicles. *IEEE Access* **2023**, *11*, 96773–96783. [CrossRef]

35. Kim, M.; Joo, D.-M.; Lee, B.K. Design and Control of Inductive Power Transfer System for Electric Vehicles Considering Wide Variation of Output Voltage and Coupling Coefficient. *IEEE Trans. Power Electron.* **2019**, *34*, 1197–1208. [CrossRef]

36. Huang, C.-C.; Lin, C.-L.; Wu, Y.-K. Simultaneous Wireless Power/Data Transfer for Electric Vehicle Charging. *IEEE Trans. Ind. Electron.* **2017**, *64*, 682–690. [CrossRef]

37. Chen, W.; Liu, Z.; Liu, J.; Ye, J.; Su, H. A New Simultaneous Wireless Power and Information Transfer System With Integrated Signal Magnetic Coupler. *IEEE Trans. Ind. Electron.* **2023**, *70*, 12708–12718. [CrossRef]

38. Onar, O.C.; Campbell, S.L.; Seiber, L.E.; White, C.P.; Chinthavali, M. Vehicular Integration of Wireless Power Transfer Systems and Hardware Interoperability Case Studies. In Proceedings of the 2016 IEEE Energy Conversion Congress and Exposition (ECCE), Milwaukee, WI, USA, 18–22 September 2016; pp. 1–8.

39. *J2954_202010*; Wireless Power Transfer for Light-Duty Plug-In/Electric Vehicles and Alignment Methodology. SAE International: Warrendale, PA, USA, 2020.

40. Bentalhik, I.; Lassioui, A.; EL Fadil, H.; Bouanou, T.; Rachid, A.; EL Idrissi, Z.; Hamed, A.M. Analysis, Design and Realization of a Wireless Power Transfer Charger for Electric Vehicles: Theoretical Approach and Experimental Results. *World Electr. Veh. J.* **2022**, *13*, 121. [CrossRef]